Structural identification of electron transfer dissociation products in mass spectrometry using infrared ion spectroscopy

Jonathan Martens[1], Josipa Grzetic[1], Giel Berden[1] & Jos Oomens[1,2]

Tandem mass spectrometry occupies a principle place among modern analytical methods and drives many developments in the 'omics' sciences. Electron attachment induced dissociation methods, as alternatives for collision-induced dissociation have profoundly influenced the field of proteomics, enabling among others the top-down sequencing of entire proteins and the analysis of post-translational modifications. The technique, however, produces more complex mass spectra and its radical-driven reaction mechanisms remain incompletely understood. Here we demonstrate the facile structural characterization of electron transfer dissociation generated peptide fragments by infrared ion spectroscopy using the tunable free-electron laser FELIX, aiding the elucidation of the underlying dissociation mechanisms. We apply this method to verify and revise previously proposed product ion structures for an often studied model tryptic peptide, $[AlaAlaHisAlaArg + 2H]^{2+}$. Comparing experiment with theory reveals that structures that would be assigned using only theoretical thermodynamic considerations often do not correspond to the experimentally sampled species.

[1] Radboud University, Institute for Molecules and Materials, FELIX Laboratory, Toernooiveld 7c, 6525ED Nijmegen, The Netherlands. [2] Van 't Hoff Institute for Molecular Sciences, University of Amsterdam, Science Park 908, 1098XH Amsterdam, The Netherlands. Correspondence and requests for materials should be addressed to J.O. (email: j.oomens@science.ru.nl).

Mass spectrometry-based analysis of peptides and proteins in the bioanalytical and clinical sciences relies on the gas-phase dissociation of their molecular ions to give sequence fragments from which the original primary structure can be inferred. Sequencing by the increasingly popular electron-induced dissociation methods (ExD, such as electron capture and transfer dissociation, ECD and ETD) has recently seen rapid development and widespread application. ECD in Fourier transform ion cyclotron resonance (FT-ICR) mass spectrometry (MS)[1–3] and more recently ETD in a much broader range of mass spectrometers[4–7] constitute the two primary variations of this method. These methods have shown impressive improvements over collision-induced dissociation tandem MS, primarily in the sense that labile post-translational modifications are not detached during activation revealing their position along the backbone, and that sequence coverage is increased, making the sequencing of intact proteins in top-down strategies possible[8–12].

Electron attachment to multiply protonated peptides or proteins leads to extensive backbone fragmentation, which most often takes the form of backbone N–C_α bond cleavages to provide the c- and z-type ion series[1,2,13,14]. The process of electron-induced N–C_α bond cleavage in peptide cation radicals has been the subject of many recent experimental and theoretical studies[13,15–20]. However, the mechanisms involved in electron attachment to peptide ions, the possible role of excited electronic states, and the structural rearrangements and fragmentation reactions that can follow, remain only partially understood. Furthermore, answers to questions regarding the ratios of fragment ions produced and their structures, especially the odd electron fragments, remain, at least partially, elusive. This is undoubtedly related to the uncertainty in the detailed nature of the (open-shell) dissociation products. For example, ExD product ions are known to undergo hydrogen atom migration reactions that increase/decrease the expected masses of the fragment ions, having direct practical implications for ExD-based sequencing applications[21,22].

Several reaction mechanisms have been proposed for ExD of which the Cornell mechanism from the group of McLafferty[2] and the more recent Utah-Washington (UW) mechanism from the groups of Tureček and Simons[19,23–25] are best known. Frison et al.[26] have discussed the different structures of c-type fragments that would result from different ECD mechanisms and were able to spectroscopically identify an amide c-type ion. While not being able to exclude the possibility that this structure results from a rearrangement after the ECD process, this assignment appears to support the UW mechanism, rather than mechanisms that would directly produce enol-imine c-type ions.

In ExD dissociation, the radical is typically on the z-type fragment, although H-atom migration reactions in the dissociating molecule may transfer the radical to the c-type fragment, resulting in changes in the m/z values of the fragments and complicating the interpretation of ExD MS/MS data. As a result, apparent unit mass shifts of backbone sequence ions in ExD spectra are thus not rare and result in an increased occurrence of ions with overlapping masses. As an illustration, for a peptide with the sequence AlaAlaHisAlaArg, hydrogen atom migration to the open-shell $z_3^{\bullet+}$ fragment would give a closed-shell z_3^+ ion having the same chemical formula as the c_4^+ fragment and makes this mass peak unassignable for sequencing purposes.

Unfortunately, the detailed information about an ion's molecular structure is scarce and often undecipherable from MS/MS data alone. Infrared spectroscopy allows the structural characterization of both the trapped precursor and fragment ions. Infrared ion spectroscopy (IRIS) has been used extensively to determine the gas-phase structures of molecular ions in MS, and specifically in the effort to elucidate peptide fragmentation mechanisms involved in collisional dissociation[27–34]. Tunable infrared free-electron lasers (FELs), such as FELIX at our institute[35], have played an important role in the recent development of IRIS[36], and are especially useful to obtain fingerprint infrared spectra of ionic species on commercial MS platforms[37]. However, to date, only a single example of infrared spectroscopy on ECD-generated fragments has been reported, in which a small closed-shell c-type ion was examined[26].

Structural characterization of peptidic ExD product ions is something that has been highly sought after for a number of years using a variety of methods, including collisional activation[38,39], ion mobility methods[40] and more recently ultraviolet photo-dissociation studies[41–43]. However, in comparison with infrared spectroscopy these methods provide limited information, regarding the structure and conformation of gas-phase ions. Structural characterization of the dissociation products by infrared spectroscopy and quantum chemistry provides a stringent test to ascertain and confirm uncertain aspects of the fragmentation mechanisms and allows for additional information to be extracted from MS/MS data. Here we present the first direct structural characterization of ETD-generated fragments using IRIS and demonstrate the strengths of this technique for addressing the questions surrounding gas-phase peptide radicals.

Results

ETD MS/MS of [AAHAR + 2H$^+$]$^{2+}$. The ETD MS/MS spectrum of the [AAHAR + 2H]$^{2+}$ (263 m/z) ion is presented in red in Fig. 1. We have characterized each of the $z^\bullet$-type fragments (depicted in the peptide sequence shown in Fig. 2) from the ETD MS/MS spectrum using infrared spectroscopy, providing a comprehensive identification of their structures and conformations. This detailed characterization forms a basis for analysing the reactions, leading to their formation.

Tryptic peptides of the AAXAR type and their ETD MS/MS behaviour have been extensively studied previously[39,42,44–47]. Here, consistent with previously reported results, we observe that fragment ion intensity is approximately split over the charge reduced ion (ETnoD) and $z^\bullet$-type sequence ions (Supplementary Fig. 1). For AAHAR, having arginine in the C-terminal position, it is not surprising that C-terminal $z^\bullet$-type fragments primarily retain the proton after dissociation and that they are the principle
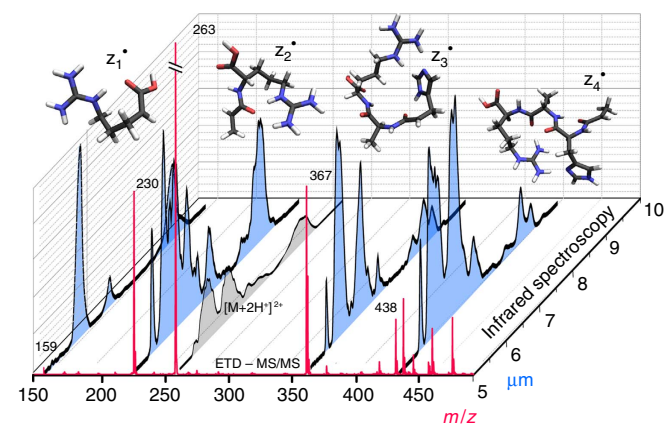

Figure 1 | The ETD MS/MS spectrum of [AAHAR + 2H]$^{2+}$ with the corresponding infrared spectra. The infrared spectra of the ETD-generated fragments are shown in black/blue and that of the precursor peptide in black/grey. Supplementary Fig. 1 contains the comprehensive ETD MS/MS results.
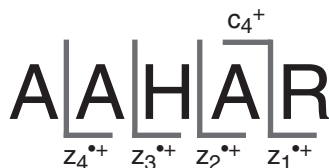
Figure 2 | Dissociation scheme and notation used for product ions. c- and z-type peptide fragments typically result from ETD MS/MS. Here we label only the discussed sequence ions from ETD of $[AAHAR+2H]^{2+}$. Note that fragments carrying a '•' symbol are open-shell radicals and those without are closed shell.
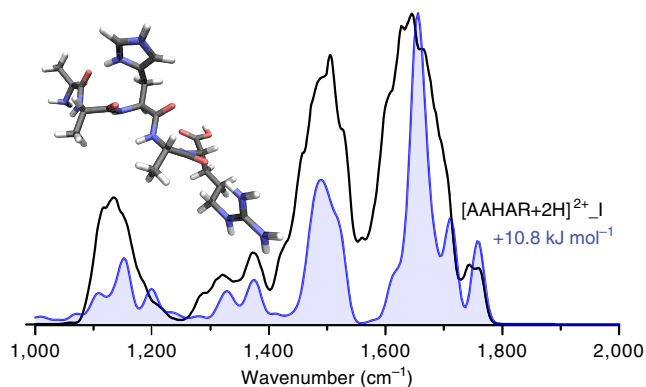

Figure 3 | The infrared spectrum of $[AAHAR+2H]^{2+}$ 263 m/z. The experimental spectrum is presented in black and the spectrum of the assigned calculated structure from this study is shown in blue along with the structure and relative free energy at 298 K.

Table 1 | Summary of structural properties and relative free energies for selected calculated structures.

	m/z	His tautomer	Radical	Rel. ΔG (kJ mol^{-1})
$[AAHAR+2H^{+}]^{2+}$	263			
I		—	—	+10.8*
II		—	—	0.0
$z_1^{\bullet+}$	159			
I		—	α	+5.4*
II		—	δ (Arg)	0.0
III		—	β (Arg)	+10.1
IV		—	γ (Arg)	+14.7
$z_2^{\bullet+}$	230			
I		—	α	0.0*
II		—	α	+10.2
III		—	δ (Arg)	+26.5
$z_3^{\bullet+}$	367			
I		N3	α	+22.4*
II		N1	α	0.0
III		N3	β (His)	0.0
$z_4^{\bullet+}$	438			
I		N3	α	0.0*
II		N3	α	+62.5
III		N3	—	+54.4
IV		N3	β (His)	+5.7
z_3^{+}	368			
I		N1	—	+28.5*
c_4_I		—	—	—
II		N3	—	0.0

Rel., relative.
An asterisk (*) indicates the structure assigned spectroscopically.

fragments in the ETD MS/MS spectrum. The electron attachment process is no doubt affected by the protonation sites and conformation of the parent peptide. In its doubly protonated state, this peptide has been shown to protonate on the imidazole group of the histidine side chain and the guanidine group of the arginine side chain[45], and our spectroscopic data and calculations confirm this.

Structure of $[AAHAR+2H^{+}]^{2+}$ precursor peptide at m/z 263. Figure 3 presents the infrared spectrum obtained for the doubly protonated peptide $[AAHAR+2H]^{2+}$ at m/z 263. Comparison with the calculated spectrum (blue) allows assignment of the protonation sites (His and Arg sidechains) and the conformation to be made. The band just <1,800 cm^{-1} is consistent with the free (or weakly H-bonded) carboxyl group. Both charged sites are hydrogen bound to backbone carbonyl groups. In terms of hydrogen bonding, involving the charged sites and the C and N termini, this assignment confirms a previously proposed structure[44], although it has an overall more extended conformation, easily distinguished by comparison with the infrared spectra (Supplementary Fig. 2).

For singly charged fragments retaining the His residue, the imidazole ring can tautomerize (having the H on either the N1 or N3 position) and we address this issue for the $z_3^{\bullet+}$ and $z_4^{\bullet+}$ fragments. Note that all fragments carrying a '•' symbol are open-shell radicals and those without are closed shell, where H's and electrons are implicit. Backbone sequence fragments studied here with the structural identification based on our spectroscopic results, as detailed in the following are summarized in Table 1.

$z_1^{\bullet+}$ fragment structure. The $z_1^{\bullet+}$ fragment is the smallest C-terminal fragment obtained upon ETD of the precursor peptide. Calculated structure $z_1^{\bullet}\_I$ was identified to match most closely with experiment, as demonstrated in the top panel of Fig. 4. This structure is the lowest-energy calculated structure from our selection of ∼30 structures from the molecular dynamics (MD) procedure. In structure $z_1^{\bullet}\_I$, the radical is located at the α-carbon adjacent to the C terminus and the carboxyl C=O stretch is found at 1,635 cm^{-1}. On the basis of this structure, radicals at other positions along the carbon chain of this fragment were defined and optimized, most of which were higher in energy. H-atom migration to the δ-carbon of the Arg side chain gave a structure 5.4 kJ mol^{-1} more stable; however, a calculated barrier of 115.2 kJ mol^{-1} (Supplementary Fig. 3) must be overcome to reach it and it is not consistent with the experimental infrared spectrum. Barriers of >100 kJ mol^{-1} for H-atom migrations have been reported for different ETD fragments[39,48,49]. With the radical in the α-position, conjugation with the carbonyl occurs giving partial double-bond character to the CC-bond, while lowering the bond order of the carbonyl, causing a significant red shift of its stretching mode relative to a carbonyl stretch >1,700 cm^{-1} in the β-, γ- and δ-radicals (Supplementary Fig. 4). This is a clear demonstration that the position of the radical can strongly influence the vibrational spectrum, in this case the C=O stretch, highlighting the value of infrared spectroscopy for characterizing open-shell peptide fragments.

$z_2^{\bullet+}$ fragment structure. Figure 5 and Supplementary Fig. 5 present infrared spectra for the $z_2^{\bullet+}$ fragment from ETD of
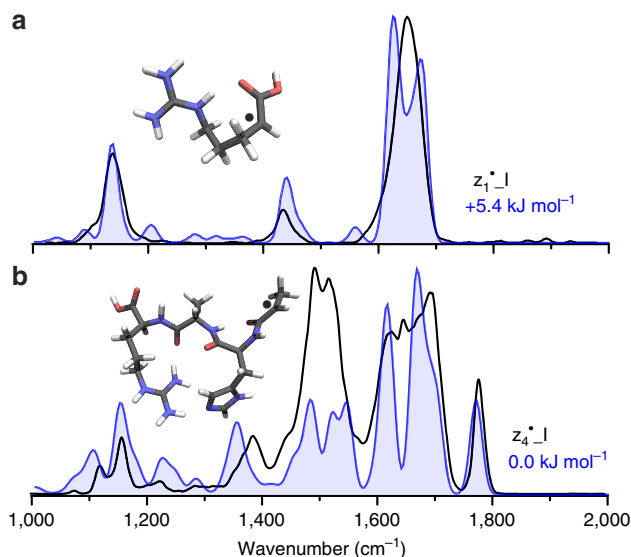
Figure 4 | The infrared spectra of the $z_1^{\bullet+}$ and $z_4^{\bullet+}$ fragments from ETD of $[AAHAR+2H]^{2+}$. The experimental spectra are presented in black in both cases and assigned calculated structures are shown in blue for (**a**) the $z_1^{\bullet+}$ fragment and (**b**) the $z_4^{\bullet+}$ fragment. The associated relative free energies (298 K) and structures are inlayed with the radical sites labelled by '•'.

Figure 5 | The infrared spectrum of the $z_2^{\bullet+}$ fragment from ETD of $[AAHAR+2H]^{2+}$. The experimental spectrum is presented in black and is compared with computed spectra for different low-energy structures. (**a**) The calculated spectrum for the assigned structure is shown in blue. (**b,c**) The calculated spectra for structures disregarded on the basis of spectral mismatch are shown in red. Calculated structures and relative free energies (298 K) are inlayed for each plot.

$[AAHAR+2H^+]^{2+}$. The calculated spectrum of $z_2^{\bullet}$_I, presented in the top panel, matches the experimental spectrum well. This structure is the lowest-energy calculation obtained from our computational procedure. A previously proposed structure[39], labelled here as $z_2^{\bullet}$_II and presented in the centre panel, closely resembles $z_2^{\bullet}$_I. However, the alternate hydrogen bonding orientation of the C terminus is distinguished by comparison with experimental and calculated infrared spectra in the 1,300–1,400 cm^{-1} region and the carbonyl stretching region just < 1,800 cm^{-1}. This refinement of the conformation reduces the relative energy by 10.2 kJ mol^{-1}. The bottom panel in the figure shows a comparison with the infrared spectrum calculated for the product of hydrogen migration from the α-carbon of the Ala residue to the δ-carbon of the Arg residue, a species 26.5 kJ mol^{-1} higher in energy and readily distinguishable spectroscopically.

$z_3^{\bullet+}$ fragment structure. Figure 6 presents the infrared spectrum for the $z_3^{\bullet+}$ fragment from ETD of $[AAHAR+2H^+]^{2+}$ with the spectrum of the assigned calculated structure $z_3^{\bullet}$_I in blue and spectra of unassigned alternative structures in red. This assignment was made after considering different conformers, imidazole tautomers and products, resulting from hydrogen atom migration interconverting between the α-radical and the β-radical on the His side chain. A low-energy His N1 tautomer ($z_3^{\bullet}$_II) was identified to be 22.4 kJ mol^{-1} lower in energy than $z_3^{\bullet}$_I, a His N3 tautomer; however, the calculated spectrum of this species does not match as well to the experiment, especially in the 1,200–1,400 cm^{-1} region (and the 3400–3600 cm^{-1} region displayed in Supplementary Fig. 6). Furthermore, a β-radical structure ($z_3^{\bullet}$_III) was found to be 22.4 kJ mol^{-1} more stable, but we do not assign this species on the basis of its spectral mismatch (Fig. 6 and Supplementary Fig. 6). The majority of stable structures we identified for each structure/tautomer of the $z_3^{\bullet+}$ ion features a stabilizing hydrogen bonding interaction between the imidazole side chain of His and the guanidinium side chain of Arg, leaving little flexibility for the orientation of the carboxyl group and giving a free C–OH group and a
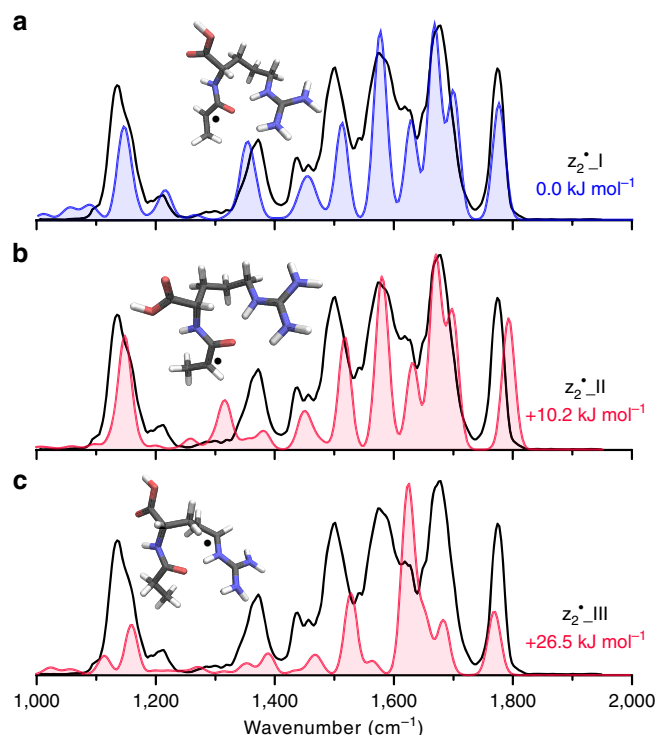
C = O weakly hydrogen bonded to the adjacent amide N–H. Being very sensitive to local environment, the position of the carboxyl C = O stretch just < 1,800 cm^{-1} can be used as a diagnostic signature. Structures $z_3^{\bullet}$_II and $z_3^{\bullet}$_III feature hydrogen bonds between the imidazole nitrogen and hydrogens of the two primary nitrogens of the guanidinium group, while in $z_3^{\bullet}$_I the hydrogen bond of the imidazole nitrogen is shared between the hydrogens of the secondary nitrogen and one primary nitrogen.

$z_4^{\bullet+}$ fragment structure. The bottom panel of Fig. 4 presents the infrared spectrum for the $z_4^{\bullet+}$ fragment from ETD of $[AAHAR+2H^+]^{2+}$ and the assigned calculated structure (blue). This is the overall lowest-energy structure obtained after an extensive MD-based search over different conformers for various tautomers and structures obtained by hydrogen migration from the α-radical to the His β-radical (see comparison of $z_4^{\bullet}$_IV in Supplementary Fig. 7). Similar to $z_3^{\bullet}$_I, the assigned structure, $z_4^{\bullet}$_I, has a hydrogen bond between the imidazole side chain and the guanidinium group of the Arg residue. Structure $z_4^{\bullet}$_I offers a refinement over a previously proposed structure[39] (here, re-optimized at the currently applied level of theory), giving both a better spectral match (see $z_4^{\bullet}$_II in Supplementary Fig. 7) and being ~ 60 kJ mol^{-1} lower in energy.

Fragment ion at m/z 368 can be z_3^+ or c_4^+. While inter- and intramolecular (between c and z fragment pairs) hydrogen migration reactions are commonly observed in ETD MS/MS, their behaviour is still relatively weakly understood. For $[AAHAR+2H^+]^{2+}$, only for the $z_3^{\bullet+}$ cation do we observe an
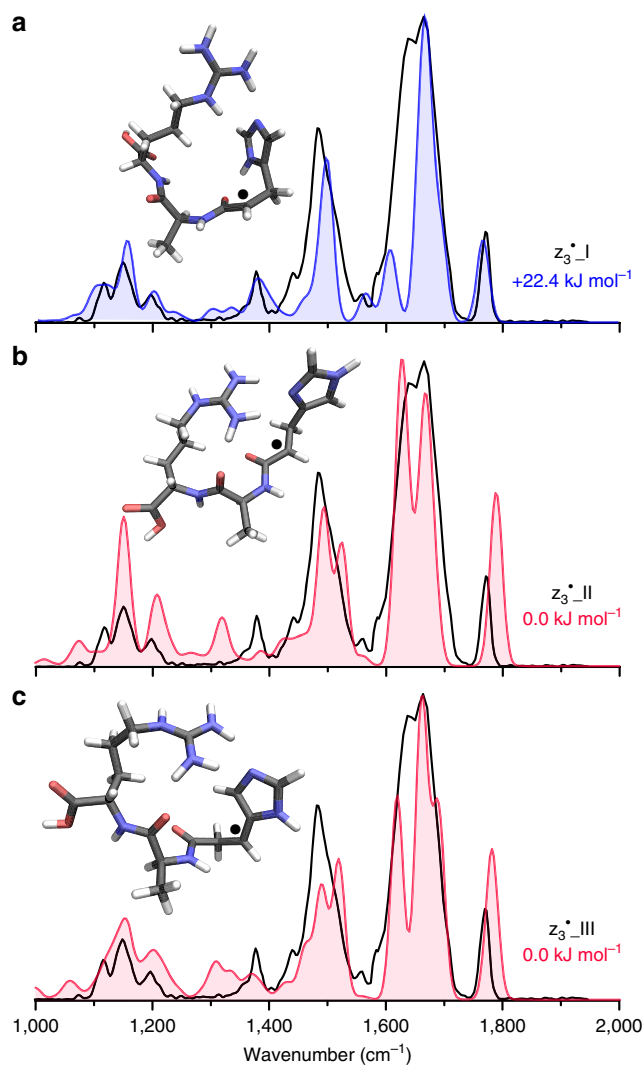
Figure 6 | The infrared spectrum of the $z_3^{\bullet+}$ fragment from ETD of [AAHAR + 2H]$^{2+}$. The experimental spectrum is presented in black and is compared with computed spectra for different low-energy structures. (**a**) The calculated spectrum for the assigned structure is shown in blue. (**b,c**) The calculated spectra for structures disregarded on the basis of spectral mismatch are shown in red. Calculated structures and relative free energies (298 K) are inlayed for each plot.
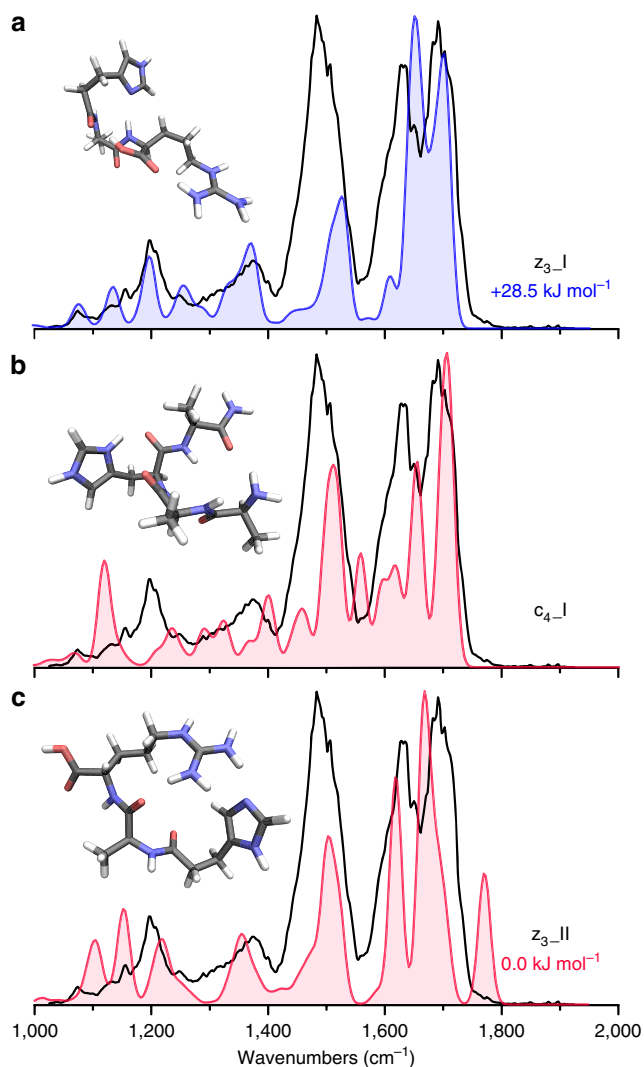

Figure 7 | The infrared spectrum of the *m/z* 368 fragment from ETD of [AAHAR + 2H]$^{2+}$. The experimental spectrum is presented in black and is compared with computed spectra for different low-energy structures. (**a**) The spectrum of the assigned calculated closed-shell z_3^+ structure is shown in blue with the structure and relative free energy (298 K) inlayed. (**b**) c_4_I is a low-energy c_4^+ conformation and its calculated infrared spectrum is presented in red. (**c**) z_3_II is the lowest energy calculated z_3^+ structure identified in this work.

appreciable extent of such a reaction, where we see both the open-shell $z_3^{\bullet+}$ fragment (*m/z* 367) and a closed-shell z_3^+ fragment (*m/z* 368). Highlighting the complications that can arise from hydrogen atom migrations in ETD, the c_4^+ fragment ($C_{15}N_7H_{25}O_4$) has the same chemical formula and overlaps the closed-shell z_3^+ fragment also at *m/z* 368. Identification and consideration of the hydrogen migration products (loss/gain) are important for assigning fragment ions and correct sequencing[38].

In Fig. 7, we identify the *m/z* 368 fragment ion as the z_3^+ species (z_3_I) based on infrared spectral matching. This structure features an alternative hydrogen bonding arrangement in comparison with the open-shell $z_3^{\bullet+}$ and $z_4^{\bullet+}$ fragments described above, most significantly affecting the C terminus (trans configuration) and red shifting the carboxyl C=O stretch for z_3_I away from the position just $<1,800\,cm^{-1}$ for the open-shell $z_3^{\bullet+}$ and $z_4^{\bullet+}$ fragments. A closed-shell equivalent of the geometry of the open-shell $z_3^{\bullet}\_I$ structure is defined as z_3_II and is 28.5 kJ mol^{-1} lower in energy than z_3_I. Calculated spectra

for structure z_3_II and c_4_I, a low-energy c_4^+ conformation, are presented in the bottom two panels of Fig. 7 and support the assignment of z_3_I.

Discussion

These results demonstrate the first use of IRIS to characterize the structures of ETD-generated peptide fragments. Using a model tryptic pentapeptide, precursor ion conformation has been related to the observed ETD fragmentation pattern, and the structures and conformations of the various fragment ions. We show that it is possible to distinguish both conformational details and different radical species, when this approach is combined with routine computational modelling.

We conclude that if structural assignments were made only on the basis of theoretical (thermodynamic) considerations, these assignments would in many cases not match the species observed in experiment—highlighting the potential for IRIS to

diagnostically identify gas-phase organic radicals and, more specifically, the mechanisms associated with peptide fragmentation in electron attachment methods. Our results suggest that hydrogen atom transfer necessary for radical migration often does not occur after ETD (without additional activation), leading to the frequent observation of non-equilibrium product ions. Understanding intermolecular hydrogen atom migration is also of practical importance, as it causes shifts in ETD fragment masses and makes sequence ion assignments more complicated.

Methods

Ion spectroscopy in a modified ion trap mass spectrometer. The experiment is based on a commercial quadrupole ion trap mass spectrometer (Bruker, AmaZon Speed ETD) coupled to the infrared beam line of the FELIX FEL. $[M + 2H]^{2+}$ peptide ions are generated by electrospray ionization. AAHAR (GeneCust (Luxemburg), 95% purity) solutions of 10^{-5}–10^{-6} mol l^{-1} (in 50:50 acetonitrile:water, $\sim 1\%$ formic acid) are introduced at 120 µl h^{-1} flow rates and desolvated by a pressurized nebulizing gas (N_2). The key hardware modifications to the instrument providing optical access to the ion population in the trap were the introduction of a new ring electrode having 3 mm holes at its top and bottom, the installation of mirrors below the trap to direct the beam back out of the instrument and optical windows in the vacuum housing. In ETD experiments, ions were accumulated for 0.1–15 ms in the trap, mass isolated and then reacted with fluoranthene radical anions for ~ 250 ms. A fragment ion of interest was mass isolated in a subsequent MS/MS stage and irradiated by the tunable infrared beam from the FEL. In the experiments reported here, the FELIX FEL was set to produce infrared radiation in the form of 5–10 µs macropulses at 5 or 10 Hz and of 30–60 mJ (bandwidth $\sim 0.4\%$ of the centre frequency). Resonant absorption of infrared radiation leads to an increase in the internal energy of the molecule aided by intramolecular vibrational redistribution of the absorbed energy. When a sufficient number of photons is absorbed (here, typically in a single macropulse), unimolecular dissociation occurs and produces frequency-dependent fragment ion intensities in the mass spectrometer (Supplementary Note 1). Relating the parent and fragment ion intensities in the observed mass spectral data (yield = ΣI(fragment ions)/ΣI(parent + fragment ions)) generates an infrared vibrational spectrum. The yield at each infrared point is obtained from averaged mass spectra and is linearly corrected for laser power; the frequency is calibrated using a grating spectrometer.

Computational chemistry. We have employed a molecular mechanics (MM)/MD approach using AMBER 12 (refs 50,51). Molecular structures manually defined based on chemical intuition where first optimized for each ion at the B3LYP/6–31 $+ +$ G(d,p) level in Gaussian09 (ref. 52). Restrained electrostatic potential (RESP) charges from these initial results were used for parameterization of the nonstandard peptide ions in the antechamber program. After minimization within AMBER, a simulated annealing procedure up to 1,000 K was used with a 1 fs step size. Five hundred structures were obtained as snapshots throughout the procedure and after MM minimization were grouped based on structural similarity using *prtraj* in AMBER. Of these, 30–50 unique structures were then each optimized at the B3LYP/6–31 $+ +$ G(d,p) level[51,53,54] and vibrational spectra were calculated within the harmonic oscillator model (vibrational frequencies were scaled by 0.975). This computational approach was applied to all structural isomers considered for each ion, except for the small $z_1^{\bullet +}$ ion, where the MM/MD conformational search was only applied once using the alpha-radical species. Calculated line spectra were broadened using a Gaussian function with a full-width at half-maximum of 25 cm^{-1} to facilitate comparison with experiment. Additional calculations using the LC-BLYP and M06 functionals for a selection of $z_1^{\bullet +}$ and $z_2^{\bullet +}$ structures, and ab initio MP2 calculations for the $z_1^{\bullet +}$ structures were performed to verify the validity of the choice of functional[49,55] and these results are summarized in Supplementary Table 1 and Supplementary Fig. 8. In general, vibrational frequencies were found to be best modelled at the B3LYP/6–31 $+ +$ G(d,p) level and calculated free energies are mostly consistent between these levels of theory. Supplementary Data 1–4 contain optimized geometries of the assigned z-type fragments.

Data availability. The data that support the findings of this study are available from the corresponding author upon request.

References

1. Kruger, N. A., Zubarev, R. A., Horn, D. M. & McLafferty, F. W. Electron capture dissociation of multiply charged peptide cations. *Int. J. Mass. Spectrom.* **185–187**, 787–793 (1999).
2. Zubarev, R. A., Kelleher, N. L. & McLafferty, F. W. Electron capture dissociation of multiply charged protein cations. a nonergodic process. *J. Am. Chem. Soc.* **120**, 3265–3266 (1998).
3. Zubarev, R. A. *et al.* Electron capture dissociation for structural characterization of multiply charged protein cations. *Anal. Chem.* **72**, 563–573 (2000).
4. Syka, J. E. P., Coon, J. J., Schroeder, M. J., Shabanowitz, J. & Hunt, D. F. Peptide and protein sequence analysis by electron transfer dissociation mass spectrometry. *Proc. Natl Acad. Sci. USA* **101**, 9528–9533 (2004).
5. Pitteri, S. J., Chrisman, P. A., Hogan, J. M. & McLuckey, S. A. Electron transfer ion/ion reactions in a three-dimensional quadrupole ion trap: reactions of doubly and triply protonated peptides with SO2●. *Anal. Chem.* **77**, 1831–1839 (2005).
6. Xia, Y. *et al.* Implementation of ion/ion reactions in a quadrupole/time-of-flight tandem mass spectrometer. *Anal. Chem.* **78**, 4146–4154 (2006).
7. Coon, J. J. *et al.* Protein identification using sequential ion/ion reactions and tandem mass spectrometry. *Proc. Natl Acad. Sci. USA* **102**, 9463–9468 (2005).
8. Swaney, D. L., McAlister, G. C. & Coon, J. J. Decision tree-driven tandem mass spectrometry for shotgun proteomics. *Nat. Meth.* **5**, 959–964 (2008).
9. Breuker, K. & McLafferty, F. W. Native electron capture dissociation for the structural characterization of noncovalent interactions in native cytochrome c. *Angew. Chem. Int. Ed.* **42**, 4900–4904 (2003).
10. Breuker, K., Oh, H., Lin, C., Carpenter, B. K. & McLafferty, F. W. Nonergodic and conformational control of the electron capture dissociation of protein cations. *Proc. Natl Acad. Sci. USA* **101**, 14011–14016 (2004).
11. Oh, H. *et al.* Secondary and tertiary structures of gaseous protein ions characterized by electron capture dissociation mass spectrometry and photofragment spectroscopy. *Proc. Natl Acad. Sci. USA* **99**, 15863–15868 (2002).
12. Breuker, K. & McLafferty, F. W. Stepwise evolution of protein native structure with electrospray into the gas phase, $10 − 12$ to 102s. *Proc. Natl Acad. Sci. USA* **105**, 18145–18152 (2008).
13. Zubarev, R. A. Reactions of polypeptide ions with electrons in the gas phase. *Mass. Spectrom. Rev.* **22**, 57–77 (2003).
14. Horn, D. M., Zubarev, R. A. & McLafferty, F. W. Automated de novo sequencing of proteins by tandem high-resolution mass spectrometry. *Proc. Natl Acad. Sci. USA* **97**, 10313–10317 (2000).
15. Tureček, F. & Julian, R. R. Peptide radicals and cation radicals in the gas phase. *Chem. Rev.* **113**, 6691–6733 (2013).
16. Simons, J. Mechanisms for S–S and N–Cα bond cleavage in peptide ECD and ETD mass spectrometry. *Chem. Phys. Lett.* **484**, 81–95 (2010).
17. Anusiewicz, I., Skurski, P. & Simons, J. Refinements to the Utah–Washington mechanism of electron capture dissociation. *J. Phys. Chem. B* **118**, 7892–7901 (2014).
18. Li, X., Lin, C., Han, L., Costello, C. E. & O'Connor, P. B. Charge remote fragmentation in electron capture and electron transfer dissociation. *J. Am. Soc. Mass. Spectrom.* **21**, 646–656 (2010).
19. Syrstad, E. A. & Tureček, F. Toward a general mechanism of electron capture dissociation. *J. Am. Soc. Mass. Spectrom.* **16**, 208–224 (2005).
20. Zhurov, K. O., Fornelli, L., Wodrich, M. D., Laskay, U. A. & Tsybin, Y. O. Principles of electron capture and transfer dissociation mass spectrometry applied to peptide and protein structure analysis. *Chem. Soc. Rev.* **42**, 5014–5030 (2013).
21. Savitski, M. M., Kjeldsen, F., Nielsen, M. L. & Zubarev, R. A. Hydrogen rearrangement to and from radical z fragments in electron capture dissociation of peptides. *J. Am. Soc. Mass. Spectrom.* **18**, 113–120 (2007).
22. Liu, J., Liang, X. & McLuckey, S. A. On the value of knowing a z● ion for what it is. *J. Proteome. Res.* **7**, 130–137 (2008).
23. Sobczyk, M. *et al.* Coulomb-assisted dissociative electron attachment: application to a model peptide. *J. Phys. Chem. A* **109**, 250–258 (2004).
24. Anusiewicz, I., Berdys-Kochanska, J. & Simons, J. Electron attachment step in electron capture dissociation (ECD) and electron transfer dissociation (ETD). *J. Phys. Chem. A* **109**, 5801–5813 (2005).
25. Chen, X. & Tureček, F. The arginine anomaly: arginine radicals are poor hydrogen atom donors in electron transfer induced dissociations. *J. Am. Chem. Soc.* **128**, 12520–12530 (2006).
26. Frison, G. *et al.* Structure of electron-capture dissociation fragments from charge-tagged peptides probed by tunable infrared multiple photon dissociation. *J. Am. Chem. Soc.* **130**, 14916–14917 (2008).
27. Lucas, B. *et al.* Investigation of the protonation site in the dialanine peptide by infrared multiphoton dissociation spectroscopy. *Phys. Chem. Chem. Phys.* **6**, 2659–2663 (2004).
28. Erlekam, U. *et al.* Infrared spectroscopy of fragments of protonated peptides: direct evidence for macrocyclic structures of b5 ions. *J. Am. Chem. Soc.* **131**, 11503–11508 (2009).
29. Bythell, B. J., Erlekam, U., Paizs, B. & Maître, P. Infrared spectroscopy of fragments from doubly protonated tryptic peptides. *Chemphyschem* **10**, 883–885 (2009).
30. Polfer, N. C., Oomens, J., Suhai, S. & Paizs, B. Spectroscopic and theoretical evidence for oxazolone ring formation in collision-induced dissociation of peptides. *J. Am. Chem. Soc.* **127**, 17154–17155 (2005).

31. Polfer, N. C., Oomens, J., Suhai, S. & Paizs, B. Infrared spectroscopy and theoretical studies on gas-phase protonated leu-enkephalin and its fragments: direct experimental evidence for the mobile proton. *J. Am. Chem. Soc.* **129,** 5887–5897 (2007).

32. Polfer, N. C. & Oomens, J. Vibrational spectroscopy of bare and solvated ionic complexes of biological relevance. *Mass. Spectrom. Rev.* **28,** 468–494 (2009).

33. Yoon, S. H. *et al.* IRMPD spectroscopy shows that agg forms an oxazolone b2+ ion. *J. Am. Chem. Soc.* **130,** 17644–17645 (2008).

34. Perkins, B. R. *et al.* Evidence of diketopiperazine and oxazolone structures for ha b2+ ion. *J. Am. Chem. Soc.* **131,** 17528–17529 (2009).

35. Oepts, D., van der Meer, A. F. G. & van Amersfoort, P. W. The free-electron-laser user facility FELIX. *Infrared Phys. Technol.* **36,** 297–308 (1995).

36. Oomens, J., Sartakov, B. G., Meijer, G. & Von Helden, G. Gas-phase infrared multiple photon dissociation spectroscopy of mass-selected molecular ions. *Int. J. Mass. Spectrom.* **254,** 1–19 (2006).

37. Bakker, J. M., Besson, T., Lemaire, J., Scuderi, D. & Maître, P. Gas-phase structure of a π-allyl − palladium complex: efficient infrared spectroscopy in a 7T Fourier transform mass spectrometer. *J. Phys. Chem. A* **111,** 13415–13424 (2007).

38. Hamidane, H. B. *et al.* Electron capture and transfer dissociation: peptide structure analysis at different ion internal energy levels. *J. Am. Soc. Mass. Spectrom.* **20,** 567–575 (2009).

39. Ledvina, A., Chung, T., Hui, R., Coon, J. & Tureček, F. Cascade dissociations of peptide cation-radicals. part 2. Infrared multiphoton dissociation and mechanistic studies of z-ions from pentapeptides. *J. Am. Soc. Mass. Spectrom.* **23,** 1351–1363 (2012).

40. Moss, C. L. *et al.* Assigning structures to gas-phase peptide cations and cation-radicals. an infrared multiphoton dissociation, ion mobility, electron transfer, and computational study of a histidine peptide ion. *J. Phys. Chem. B* **116,** 3445–3456 (2012).

41. Shaffer, C. J., Marek, A., Pepin, R., Slovakova, K. & Turecek, F. Combining UV photodissociation with electron transfer for peptide structure analysis. *J. Mass. Spectrom.* **50,** 470–475 (2015).

42. Nguyen, H. T. H., Shaffer, C. J. & Tureček, F. Probing peptide cation–radicals by near-uv photodissociation in the gas phase. structure elucidation of histidine radical chromophores formed by electron transfer reduction. *J. Phys. Chem. B* **119,** 3948–3961 (2015).

43. Nguyen, H. T. H., Shaffer, C. J., Pepin, R. & Tureček, F. U. V. Action spectroscopy of gas-phase peptide radicals. *J. Phys. Chem. Lett.* **6,** 4722–4727 (2015).

44. Tureček, F., Moss, C. L. & Chung, T. W. Correlating ETD fragment ion intensities with peptide ion conformational and electronic structure. *Int. J. Mass. Spectrom.* **330–332,** 207–219 (2012).

45. Tureček, F. *et al.* The histidine effect. electron transfer and capture cause different dissociations and rearrangements of histidine peptide cation-radicals. *J. Am. Chem. Soc.* **132,** 10728–10740 (2010).

46. Zimnicka, M., Moss, C., Chung, T., Hui, R. & Tureček, F. Tunable charge tags for electron-based methods of peptide sequencing: design and applications. *J. Am. Soc. Mass. Spectrom.* **23,** 608–620 (2012).

47. Chung, T., Hui, R., Ledvina, A., Coon, J. & Tureček, F. Cascade dissociations of peptide cation-radicals. part 1. scope and effects of amino acid residues in penta-, nona-, and decapeptides. *J. Am. Soc. Mass. Spectrom.* **23,** 1336–1350 (2012).

48. Chung, T. W. & Tureček, F. Backbone and side-chain specific dissociations of z ions from non-tryptic peptides. *J. Am. Soc. Mass. Spectrom.* **21,** 1279–1295 (2010).

49. Riffet, V., Jacquemin, D. & Frison, G. H-atom loss and migration in hydrogen-rich peptide cation radicals: The role of chemical environment. *Int. J. Mass. Spectrom.* **390,** 28–38 (2015).

50. Case, D.A. *et al.* AMBER 12 (University of California, San Francisco, CA, 2012).

51. Martens, J. K., Grzetic, J., Berden, G. & Oomens, J. Gas-phase conformations of small polyprolines and their fragment ions by IRMPD spectroscopy. *Int. J. Mass. Spectrom.* **377,** 179–187 (2015).

52. Frisch, M. J. *et al.* Gaussian 09 (Gaussian, Inc., Wallingford, CT, 2009).

53. Halls, M. D. & Schlegel, H. B. Comparison of the performance of local, gradient-corrected, and hybrid density functional models in predicting infrared intensities. *J. Chem. Phys.* **109,** 10587–10593 (1998).

54. Kapota, C., Lemaire, J., Maître, P. & Ohanessian, G. Vibrational signature of charge solvation vs salt bridge isomers of sodiated amino acids in the gas phase. *J. Am. Chem. Soc.* **126,** 1836–1842 (2004).

55. Riffet, V., Jacquemin, D., Cauët, E. & Frison, G. Benchmarking DFT and TD-DFT functionals for the ground and excited states of hydrogen-rich peptide radicals. *J. Chem. Theory. Comput.* **10,** 3308–3318 (2014).

Acknowledgements

Author contributions

J.M., G.B. and J.O. conceived and designed the experiments. J.M. and J.G. performed the experiments and computations. The manuscript was co-written by all authors.

Additional information